

An analysis of warm pool and cold tongue El Niños: air–sea coupling processes, global influences, and recent trends

Zeng-Zhen Hu · Arun Kumar · Bhaskar Jha ·
Wanqiu Wang · Bohua Huang · Boyin Huang

Received: 7 January 2011 / Accepted: 14 October 2011 / Published online: 29 October 2011
© Springer-Verlag (outside the USA) 2011

Abstract The differences in tropical air–sea interactions and global climate connection as well as the hindcast skills for the warm pool (WP) and cold tongue (CT) El Niños are investigated based on observed, (re)analyzed, and model hindcast data. The robustness of observed global climate connection is established from the model simulations. Lastly, variations of atmosphere and ocean conditions in the recent decades, and their possible connection with the frequency increase of the WP El Niño are discussed. Consistent with previous results, our individual case study and composite results suggest that stronger (weaker) and more eastward extended (westward confined) westerly wind along the equatorial Pacific in early months of a year is associated with active (suppressed) air–sea interaction over the cold tongue/the Intertropical Convergence Zone complex, as well as more (less) intensive oceanic thermocline feedback, favoring the CT (WP) El Niño development. The preceding westerly wind signal and air–sea interaction differences may be responsible for the prediction skill difference with higher (lower) overall hindcast

skill for the CT (WP) El Niño in the Climate Forecast System of National Centers for Environmental Prediction. Our model experiments show that, in addition to the tropics, the eastern Pacific, North America and North Atlantic are the major regions having robust climate differences between the CT and WP El Niños. Nevertheless, the climate contrasts seem not robust over the Eurasian continent. Also, the frequency increase of the WP El Niño in the recent decades may not be directly connected with the linear trend of the tropical climate.

1 Introduction

Sea surface temperature (SST) anomaly (SSTA) in the tropical Pacific Ocean associated with the El Niño–Southern Oscillation (ENSO) affects global climate variability on seasonal to interannual time scales. Although generally characterized by a zonal sea-level pressure (SLP) seesaw, and large SSTA from the central to eastern Pacific, as well as equatorial zonal wind and precipitation anomalies (Kumar and Hu 2011), individual ENSO events differ in their evolutionary cycle, and such differences are often referred to as “different flavors of ENSO” (Trenberth and Smith 2006). Even with short length of observational data sets, there was a tentative evidence that ENSO, and particularly its warmer phase, i.e., the El Niño, can be categorized into two classes (Weare et al. 1976; Hoerling and Kumar 2002). With the availability of longer observational data, further evidence for two preferred patterns of the El Niño SSTA has emerged. One category of El Niño has maximum warming occurring in the central equatorial Pacific. In literature, this pattern has been referred by a myriad collection of names, e.g., dateline El Niño (Larkin and Harrison 2005), El Niño Modoki (Ashok et al. 2007;

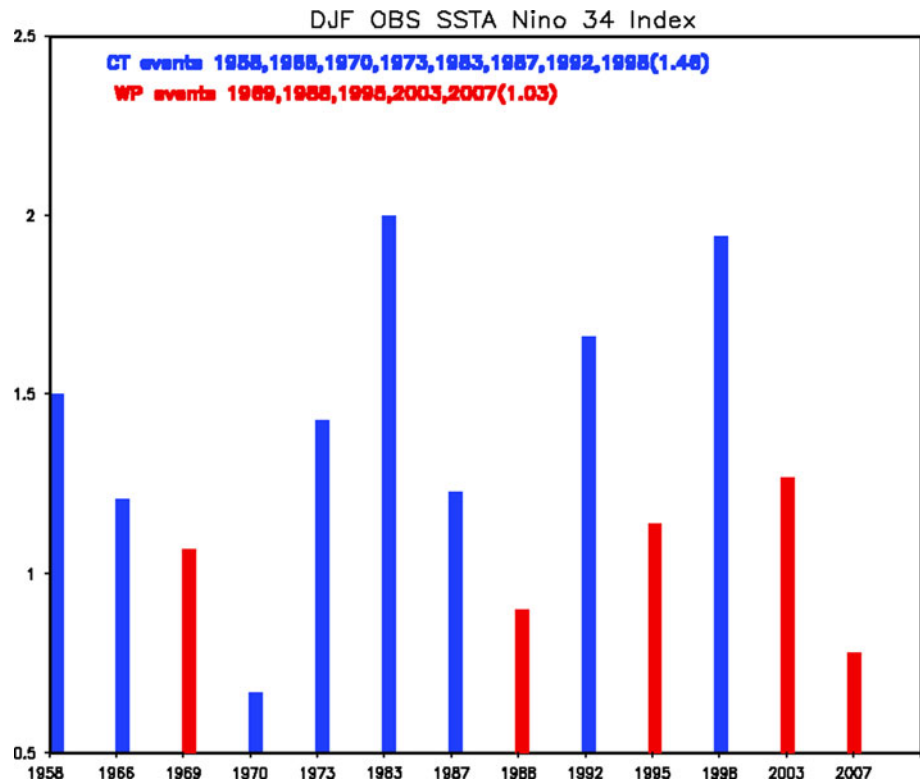
Z.-Z. Hu (✉) · A. Kumar · B. Jha · W. Wang · Boyin Huang
Climate Prediction Center, NCEP/NWS/NOAA,
5200 Auth Road (Suite 605), Camp Springs, MD 20746, USA
e-mail: Zeng-Zhen.Hu@NOAA.GOV

B. Jha · Boyin Huang
Wyle Information Systems, Camp Springs, MD 20746, USA

Bohua Huang
Department of Atmospheric, Oceanic, and Earth Sciences,
College of Science, George Mason University,
4400 University Drive, Fairfax, VA 22030, USA

Bohua Huang
Center for Ocean-Land-Atmosphere Studies,
4041 Powder Mill Road, Suite 302, Calverton, MD 20705, USA

Fig. 1 Nino3.4 values in the WP (red bar) and CT (blue bar) El Niño years during 1950–2008. The WP El Niño event is defined as $Nino4 > Nino3$ and $Nino4 > 0.5^{\circ}\text{C}$, and CT El Niño event is defined as $Nino3 > Nino4$ and $Nino3 > 0.5^{\circ}\text{C}$. Both Nino3 and Nino4 indices are calculated using ERSSTv3 SSTA in $D(-1)JF(0)$ during 1950–2008 and the El Niño years are referred to as the years of Jan. and Feb. There are 5 WP El Niño cases and 8 CT El Niño cases during 1950–2008



Weng et al. 2007, 2009), warm pool (WP) El Niño (Kug et al. 2009, 2010), or central Pacific (CP) El Niño (Yeh et al. 2009; Kao and Yu 2009; Yu and Kim 2010a, b). The other category of events is the conventional El Niño referred to as the cold tongue (CT) El Niño (Kug et al. 2009, 2010), or eastern Pacific El Niño (Yeh et al. 2009; Kao and Yu 2009; Yu and Kim 2010a, b).

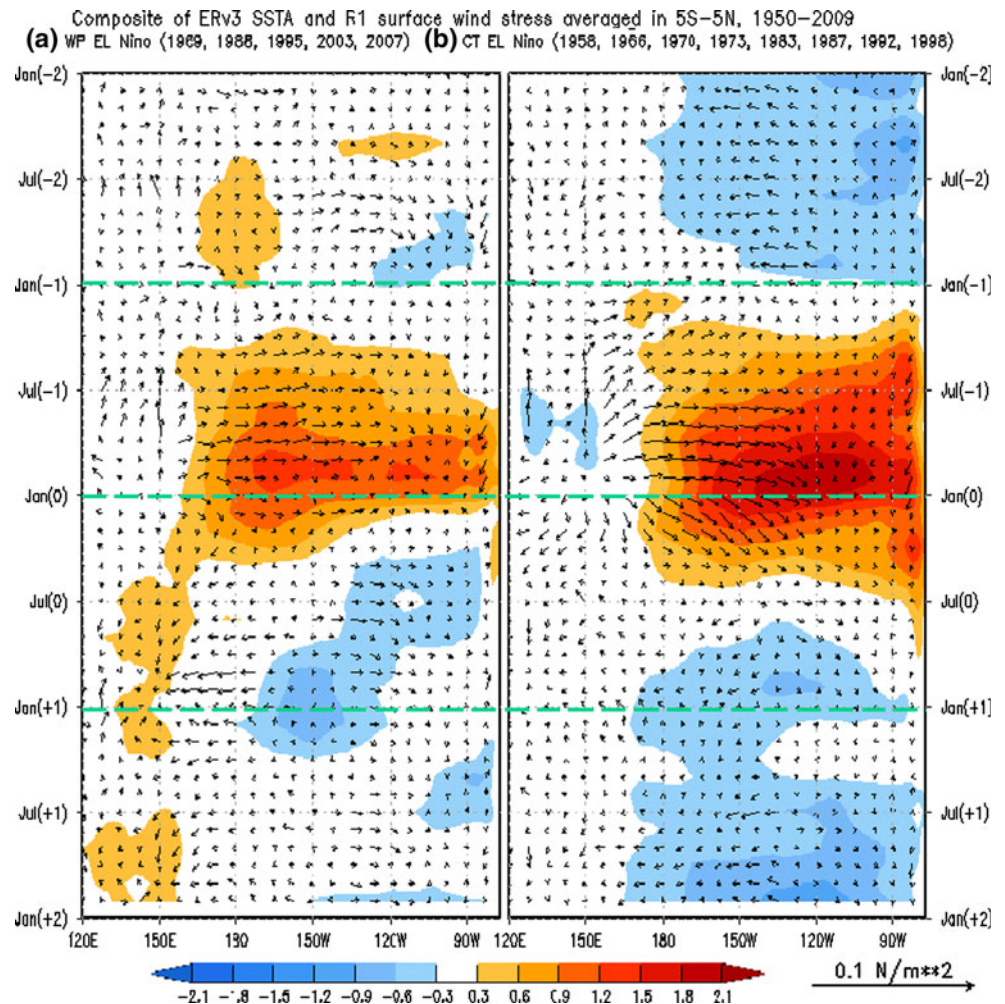
Notwithstanding different names have been used in the literature, the major SSTA in the tropical Pacific displays a similar spatial structure for two distinct categories of El Niño. For example, the SSTA pattern referred to as El Niño Modoki, WP, dateline, or CP El Niño shows opposite variations between the central equatorial and southeastern tropical Pacific. On the other hand, for the SSTA pattern referred to as conventional, CT, or EP El Niño, the maximum SSTA is present in the central and eastern Pacific. For further discussion, we adopt the WP and CT El Niños to name the two types of El Niños. Given the fact that it may be possible to categorize El Niño into two broad classes, it is important to understand their differences in the air–sea interaction processes, atmospheric response, and to assess their prediction skills, which is the focus of this paper.

The physical processes associated with the two types of El Niño are posited to relate to different coupled feedback mechanisms. For example, the CT El Niño is shown to be associated with basin wide thermocline and surface wind variations, whereas the WP El Niño with surface wind, SST, and subsurface anomalies that remain confined in the

central and western Pacific (Ashok et al. 2007; Kao and Yu 2009; Kug et al. 2009). Zonal advective feedback (i.e., zonal advection of mean SST by anomalous zonal currents) was suggested to play a crucial role for the WP El Niño, while thermocline feedback is argued to be a key process for the CT El Niño (Kug et al. 2009; Kao and Yu 2009). Recently, by analyzing the physical processes associated with the two types of El Niño in a CGCM, Kug et al. (2010) concluded that the poleward discharge of equatorial heat is stronger in the CT El Niño than in the WP El Niño. The weak discharge of the equatorial heat content associated with the WP El Niño may not be an efficient process in triggering a cold event in the post WP El Niño seasons (Kug et al. 2009). Thus, the WP El Niño may occur more as individual events instead of a preference for a cyclical nature of the CT El Niño (Kao and Yu 2009) where an El Niño is followed by a La Niña.

The two-types of El Niños may also differ in their atmospheric teleconnection patterns (Ashok et al. 2007; Weng et al. 2007, 2009; Yeh et al. 2009). For example, Ashok et al. (2007) found that, depending on the season, the impacts of the WP El Niño over regions such as the Far East Asia, New Zealand, and the western coast of United States are opposite to those of the CT El Niño. There are two mid-tropospheric wave trains passing over the extratropical and subtropical North Pacific: a positive phase of a Pacific–Japan (PJ) pattern, and a positive phase of a summertime Pacific–North American (PNA) pattern

Fig. 2 Composite of monthly mean SSTA (*shading*) and surface wind stress anomaly (vectors) averaged in 5°S–5°N for **a** 5 WP El Niño events (1969, 1988, 1995, 2003, 2007) and **b** 8 CT El Niño events (1958, 1966, 1970, 1983, 1987, 1992, 1998). The composites of SSTA and wind stress are calculated based on ERSSTv3 and R1, respectively



(Weng et al. 2007). These teleconnection patterns cause significant precipitation and surface air temperature anomalies, and differ between WP and CT El Niño (Weng et al. 2007).

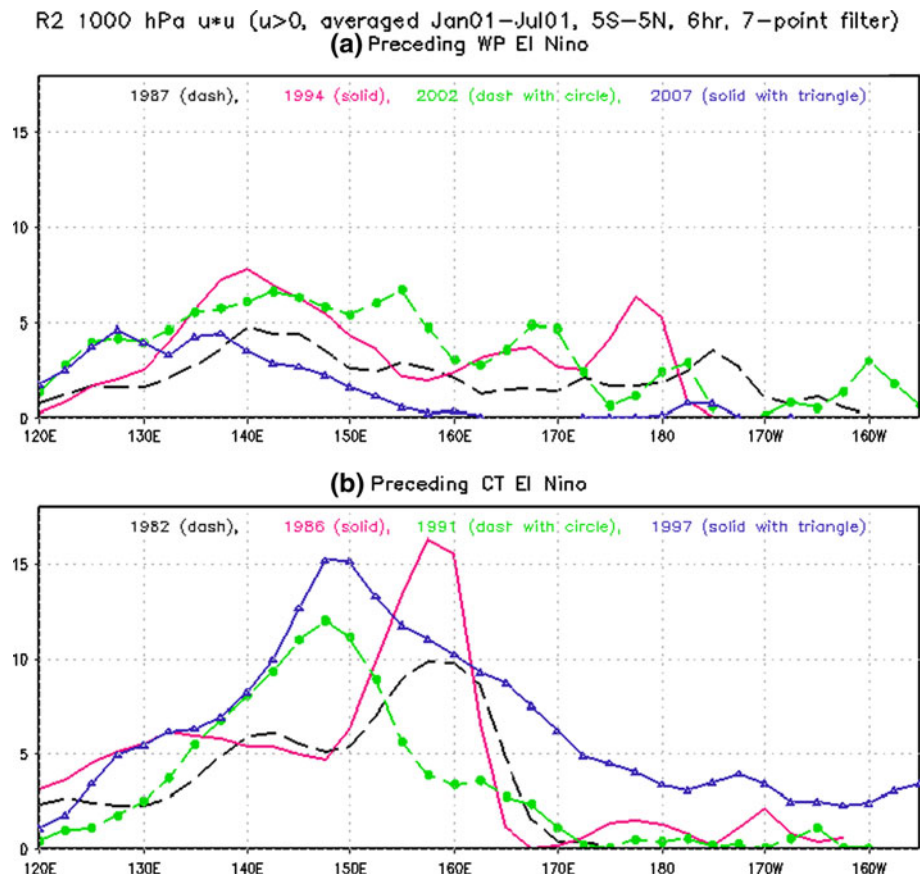
Considering lower frequency variations, e.g., on decadal time scale, the relative frequency of the WP and CT events might partly depend upon the low-frequency variations of the tropical Pacific mean state (Latif et al. 1997; Choi et al. 2011). Observations indicate that the frequency of the WP El Niño occurrence has increased (Yeh et al. 2009) and its intensity has almost doubled in the past few decades (Lee and McPhaden 2010). The observed change in frequency of the two types of El Niños was suggested to be associated with a flattening of the thermocline in the equatorial Pacific caused by a weakening of equatorial easterlies in response to the weakened zonal SST gradient (Ashok et al. 2007; Yeh et al. 2009). However, it remains an open question if changes in the characteristics of El Niño are occurring in tandem with low-frequency variations in the climate system or are merely a coincidence.

In this work, we will focus on the following topics: (1) what is the contrast in intensity and location of

preceding westerly winds associated with the air-sea interaction between WP and CT El Niños and their possible roles in affecting the subsequent patterns of air-sea interaction? (2) What are the robust differences in the atmospheric responses in the extra-tropics (as this information can be used for improving seasonal climate prediction)? (3) What are the differences in the prediction skill between the two types of El Niños in coupled general circulation models (CGCMs)? (4) Are the low frequency variation of atmosphere and ocean conditions connected with the observed changes in the ENSO characteristics, for example, the recent increase in the frequency of the WP El Niño events?

The paper is organized as follows. After describing the observational data and model simulations and hindcasts in Sect. 2, we discuss the differences of tropical air-sea interaction and the evolution of global SSTA for the WP and CT El Niño in Sect. 3. We focus on contrasting the surface winds preceding the El Niño in triggering these differences. In Sect. 4, differences in the atmospheric response to the two types of El Niños are documented

Fig. 3 u^2 for the westerly wind only averaged in 5°S – 5°N and between Jan. 1st and Jul. 1st of Year (-1) preceding El Niño development for the WP (*top*) and CT (*bottom*) El Niño years. The zonal winds are the 6 hourly data of R2, which are smoothed using 7-point running mean



using observational data and their robustness is further verified with atmospheric general circulation models (AGCM) simulations and sensitivity experiments. The hindcast skill of the two types of El Niños is also examined and possible reasons for skill differences are discussed. Through examining the long-term trends of ocean condition, we investigate the possible connection of the trends with the WP and CT El Niños in Sect. 5. A summary with some discussion is given in Sect. 6.

2 Data sources

2.1 Observational data

Monthly mean reanalysis data from Jan. 1979 to Dec. 2009 used in this work include ocean surface wind stress and SLP, and monthly and 6 hourly mean surface wind at 1,000 hPa from National Centers for Environmental Prediction (NCEP) and Department of Energy atmospheric reanalysis 2 (R2) (Kanamitsu et al. 2002a), and monthly mean ocean temperature from the Global Ocean Data Assimilation System (GODAS) (Behringer and Xue 2004). The mixed layer heat budget in the tropical Pacific is also diagnosed using data from GODAS (Huang et al. 2010).

We also use observation-based monthly mean analyses: version 3 of the extended reconstruction of the SST analyses (ERSSTv3) from Jan. 1950 to Dec. 2009 (Smith et al. 2008), version 2 of the optimum interpolation (OIv2) SST from Nov. 1981 to Dec. 2009 (Reynolds et al. 2002), CAMS-OPI precipitation from the Climate Prediction Center (CPC) from Jan. 1979 to Dec. 2009 (Janowiak and Xie 1999), land surface air temperature from the CPC CAMS from Jan. 1950 to Dec. 2009 (Ropelewski et al. 1985), ocean surface wind stress and meridional wind at 200 hPa (V200) from NCEP/National Center for Atmospheric Research (NCEP/NCAR) reanalysis 1 (R1) between Jan. 1950 and Dec. 2009 (Kalnay et al. 1996), and heat content between the ocean surface and 300 meters (HC300) from Jan. 1956 to Dec. 2009 (Levitus et al. 2009). The monthly mean HC300 was interpolated from the analysis available at a three-month mean resolution. All anomalies are computed relative to their monthly mean climatologies averaged over respective data periods.

Following Yeh et al. (2009), El Niño events during 1950–2008 are defined based on ERSSTv3 SSTA in Dec., Jan., and Feb. (DJF) averaged in Nino3.4, Nino3, and Nino4 regions (Fig. 1). An El Niño event is referred to as the WP El Niño if $\text{Nino4} > \text{Nino3}$ and $\text{Nino3.4} > 0.5^{\circ}\text{C}$ (red bars in Fig. 1), and as the CT El Niño if

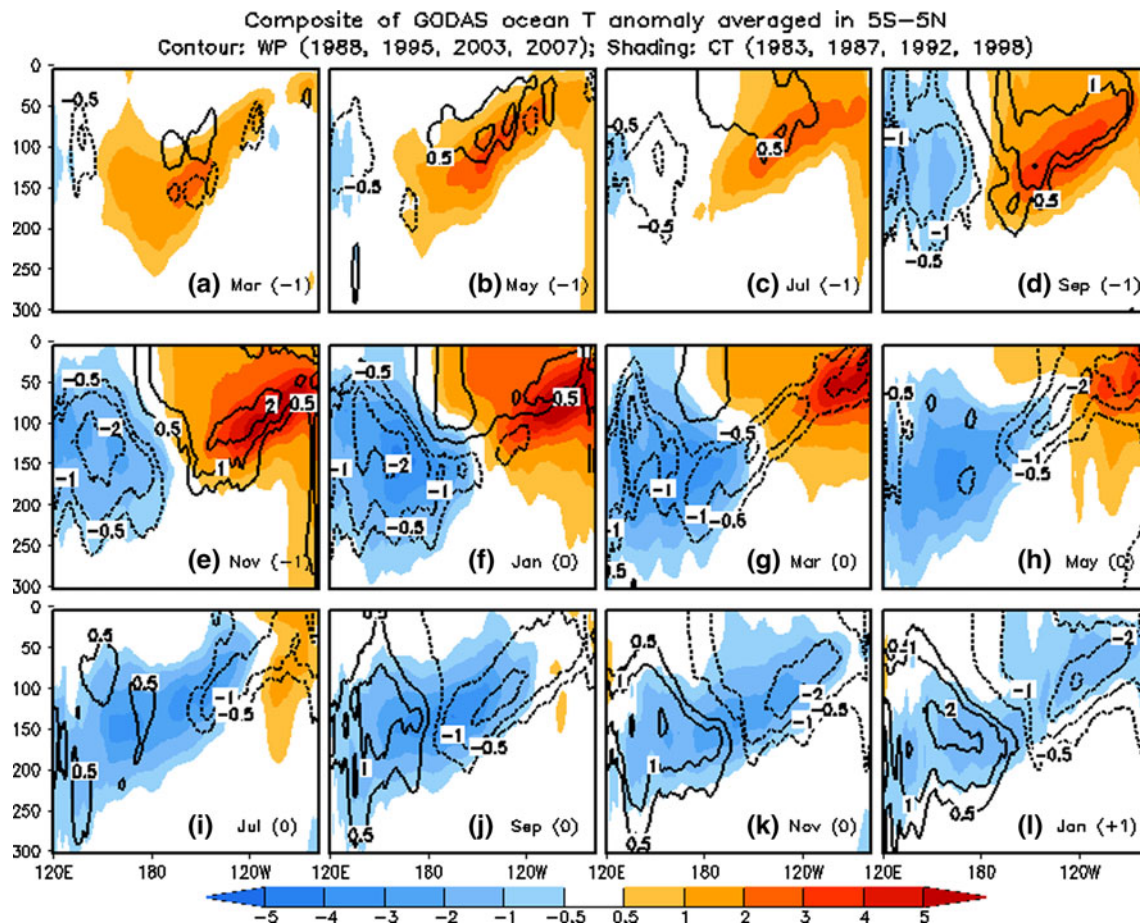


Fig. 4 Composite of monthly mean ocean temperature anomalies between the ocean surface and 300 m averaged in 5°S–5°N for 4 WP El Niño events (1988, 1995, 2003, 2007) (contour) and 4 CT El Niño

events (1983, 1987, 1992, 1998) (shading). The contours are -5 , -4 , -3 , -2 , -1 , -0.5 , 0.5 , 1 , 2 , 3 , 4 , and 5 °C

$Nino3 > Nino4$ and $Nino3.4 > 0.5$ °C (blue bars in Fig. 1). The El Niño years are referred to as the years of Jan. Based on these criteria, there are 5 WP El Niño years (1969, 1988, 1995, 2003, and 2007) and 8 CT El Niño years (1958, 1966, 1970, 1973, 1983, 1987, 1992, and 1998) during 1950–2008. From Fig. 1, it is seen that the WP El Niño events were more frequent in post 1980 period relative to prior to 1980 period, a trend noted in previous investigations (Ashok et al. 2007; Yeh et al. 2009). In the discussion of El Niño composites, “Year (0)”, “Year (+1)”, “Year (+2)”, “Year (–1)”, and “Year (–2)” represent the peak year, 1 and 2 years after the peak year, and 1 and 2 years prior to the peak year, respectively.

2.2 Model simulations and hindcasts

A suite of ensemble simulations from three AGCMs are used to evaluate the robustness of the observed atmospheric response to the two types of El Niños. The three AGCMs simulations are: 9 members from the National Aeronautics

and Space Administration (NASA) Seasonal-to-Interannual Prediction Project (NSIPP) AGCM (Bacmeister et al. 2000), 24 members from the European Centre for Medium-Range Weather Forecasts–Hamburg version climate model 4.5 (ECHAM4.5) run at the International Research Institute for Climate and Society (Roeckner et al. 2006), and 9 members from the Experimental Climate Prediction Center’s global Seasonal Forecast Model (ECPC/SFM) (Kanamitsu et al. 2002b). All the AGCMs were forced by observed SSTs and integrated from Jan. 1950 to Dec. 2009.

To further identify the robust differences, an additional set of simulations was made using the NCEP Global Forecast System (GFS), which is the atmospheric component of the NCEP Climate Forecast System (CFS, Saha et al. 2006). Two 35-year integrations were conducted with climatological mean seasonal cycle of SST plus a global SSTA for the WP and CT El Niño composites in D(–1)JF(0) (Fig. 7), respectively. The anomalies in these two integrations are computed with respect to a 35-year control run forced by climatological seasonal cycle of SST.

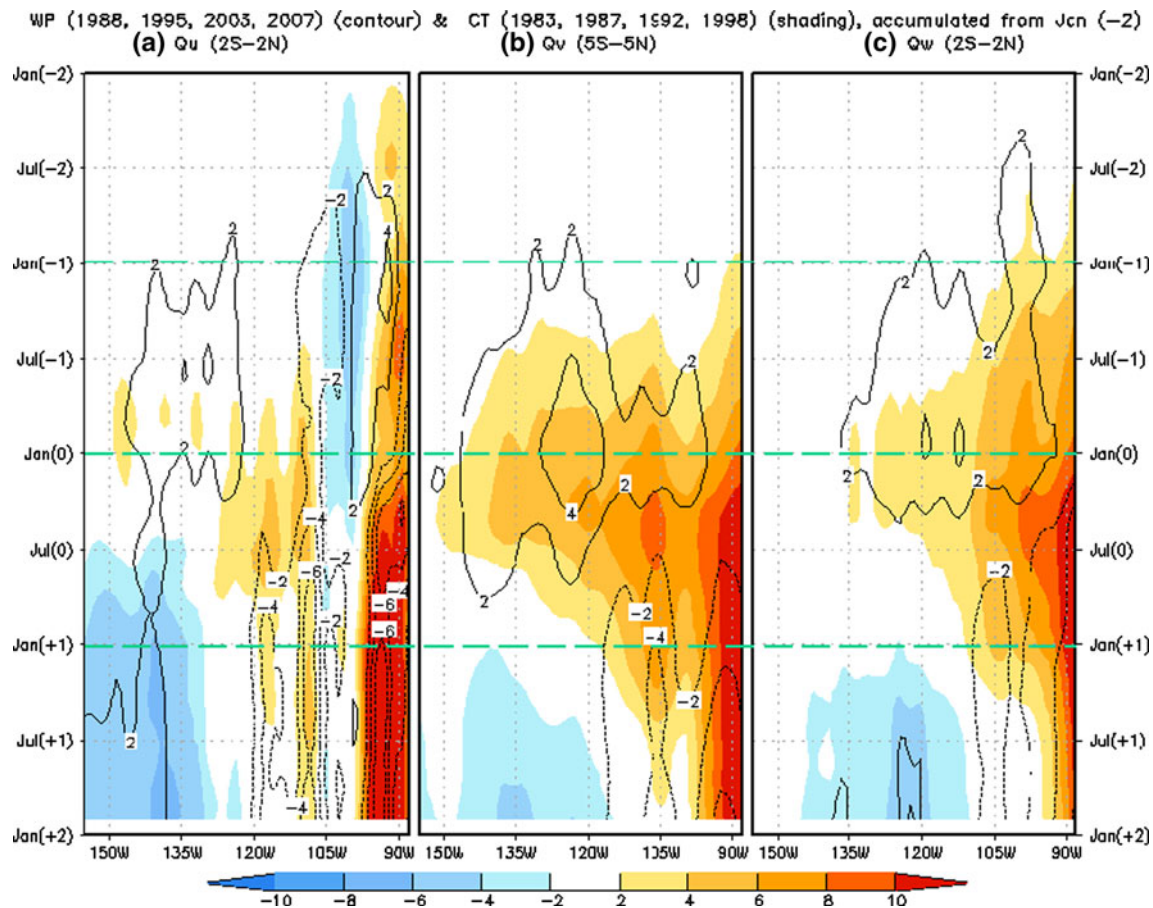


Fig. 5 Composites of time accumulated monthly mean **a** Qu averaged in 2°S – 2°N , **b** Qv averaged in 5°S – 5°N , and **c** Qw averaged in 2°S – 2°N for 4 WP El Niño events (1988, 19956, 2003, and 2007) (contour) and 4 CT El Niño events (1983, 1987, 1992, and 1998)

(shading). The accumulation starts from Jan. (-2). The contour and shading interval is 2°C . The composites are calculated based on GODAS in 1979–2009. Zero line is suppressed

The NCEP CFS hindcasts are used to assess the differences in prediction skill for the WP versus the CT El Niños, and the hindcasts were initialized in all calendar months from 1981 to 2008. For each month, 15 hindcasts of 9-month length from lead month 0 to 8 are available with different oceanic and atmospheric initial condition (IC) (Saha et al. 2006). Both the simulation and hindcast results are composited and analyzed according to the WP and CT events defined and shown in Fig. 1.

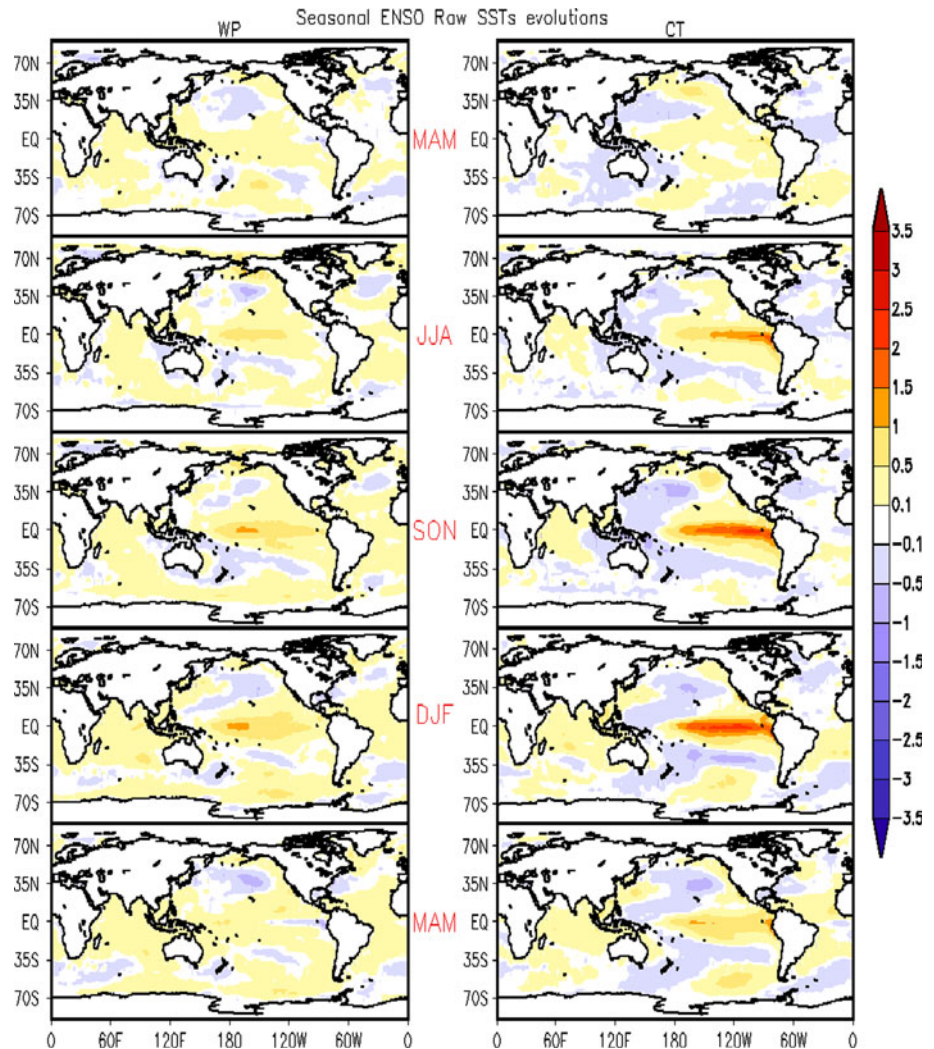
3 Evolution of the WP and CT El Niños and associated physical processes

3.1 Air–sea interaction in the tropical Pacific

SSTA and surface wind stress anomaly composites of the CT and WP El Niños along the equator (Fig. 2) shows appreciable differences in their amplitude, spatial pattern, and seasonality, generally consistent with that of previous

studies (e.g., Ashok et al. 2007; Kug et al. 2009; Kao and Yu 2009). On average, the amplitude of the WP El Niño is weaker than that of CT events with $\sim 1.2^{\circ}\text{C}$ for the former (Fig. 2a), and $\sim 2.1^{\circ}\text{C}$ for the latter (Fig. 2b). For the WP El Niño (Fig. 2a), major SSTAs are initiated in the western and central equatorial Pacific in late boreal spring, then grow and peak in late boreal fall while expanding eastward, and start to decay afterwards. By the spring of Year (0), there is practically no anomaly of either sign in the eastern Pacific. On the other hand, for the CT El Niño (Fig. 2b), major SSTAs are initiated near the eastern coast of South America in early spring, then peak in the central and eastern Pacific around 135° – 110°W with a westward propagation. The warm SSTAs in the central and eastern equatorial Pacific persist in late winter and early spring of Year (0) accompanied by persistent westerly wind anomalies from the dateline to 120°W . Moreover the WP El Niño has a shorter period than the CT El Niño. Maximum negative SSTA appears in the boreal winter of Year (+1) in the WP El Niño (Fig. 2a) while a stronger cold anomaly

Fig. 7 Seasonal mean SSTA composites for the WP (*left*) and CT (*right*) El Niño events during 1950–2008



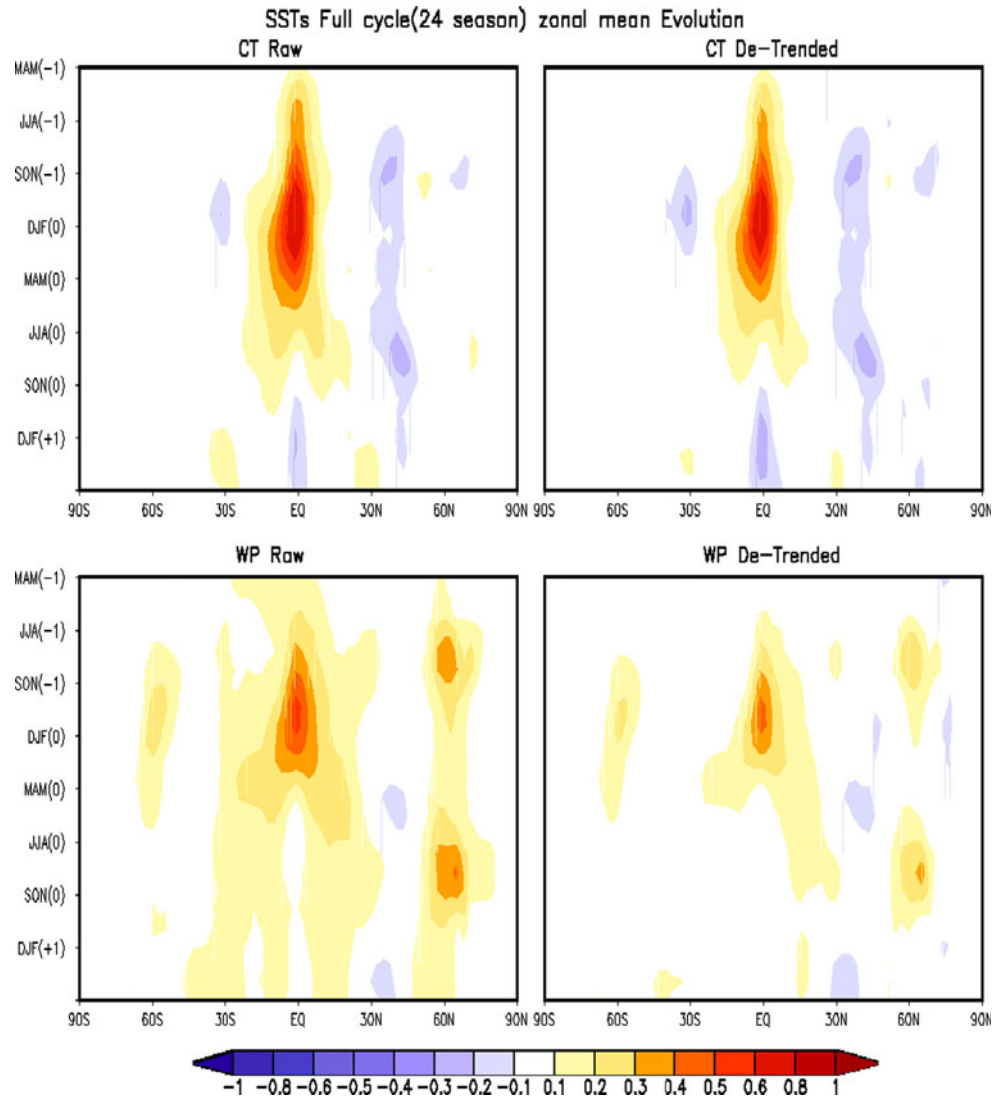
along the equator penetrates farther eastward in the former than in the latter. For example, the maximum of the WWE is located at 145–160°E for the CT El Niño and around 140°E for the WP El Niño (except 2002 with a second peak around 155°E). So, CT (WP) El Niño events are triggered by a relatively stronger (weaker) and further eastward (westward) extended (confined) westerly winds. The intensity and longitude extension of the westerly winds along the equator in early months of a year may therefore be a factor in deciding whether an El Niño event will develop into a CT or a WP El Niño event. Such contrasts may also explain the differences in perturbations along the thermocline (Fig. 4).

The GODAS ocean analysis spans the period from 1979 to 2009, which cover four WP (1988, 1995, 2003, and 2007) and four CT (1983, 1987, 1992, and 1998) El Niño events. Thus, WP and CT composites for the subsurface ocean temperature anomaly (OTA) are discussed for composites based just over these years. The composites of OTA for these two groups of events show quite different

evolution in the equatorial thermocline. During the initiation stage of the WP events (contour in Fig. 4a–c), there is only a weak warming confined in the upper part of the ocean in the central Pacific. The anomalies near the thermocline remain weak during the development of the WP events, e.g., Sep. (–1) to Nov. (–1) (Fig. 4d–e). This is consistent with Fig. 8 of Ashok et al. (2007) and Fig. 8b of Kao and Yu (2009). In contrast, deepening of the thermocline is clearly seen throughout the equatorial Pacific from the dateline starting in Mar. (–1) for the CT El Niño (shading in Fig. 4). Although the thermocline deepening can be seen in both type of El Niños from Sep. (–1) to Nov. (–1) (Fig. 4d–e), suggesting that the Bjerknes feedback (Bjerknes 1969) plays a role in both, its effect is clearly stronger for the CT events.

The contrasting evolution of the WP and CT El Niños is further analyzed based on the ocean mixed-layer heat budget. The evolution of *time accumulated* dynamical terms in mixed-layer ocean heat budget, including zonal (Q_u), meridional (Q_v), and vertical (Q_w) advectons, is

Fig. 8 Evolution of seasonal mean composites of zonally averaged SSTA for the CT (top panels) and WP (bottom panels) El Niño events during 1950–2008. Left panel is for raw data and right panel for detrended data



shown in Fig. 5 for the CT (shading) and WP CT El Niño event composite. For Q_v (Fig. 5a), the maximum is in between 150 and 120°W around Jul. (-1) for the WP El Niños, but is in between 130 and 105°W around Jul. (0) for the CT El Niños. For both Q_v and Q_w (Fig. 5b, c), the maximum presents around 125°W in Jan. (0) with amplitude of 4°C for the WP El Niños, and eastward of 110°W in Jul. (0) with much larger amplitude for the WP El Niños. The times of Q_u and Q_v maximum occurrences are in line with previous studies. For example, Huang and Schneider (1995) have suggested that the El Niño development is mainly due to advection of anomalous zonal current in the western Pacific during its initiation stage, while the meridional advection in the central Pacific, and the displacement of thermocline in the eastern Pacific become dominant during its developing and mature phases. To summarize, compared with the CT events, the horizontal and vertical advectations in the WP events are weaker and

occur earlier and further westward. This is consistent with evolution of SSTA, westerly wind, and OTA shown in Figs. 2, 3 and 4.

Interestingly, there is a major shift in the direction of the equatorial wind anomalies in the boreal winter and spring of Year (0) from westerly to northwesterly in the CT El Niño (Fig. 2b). This shift is accompanied by positive precipitation anomaly and surface anomalous convergence in the central and eastern equatorial Pacific, and negative precipitation anomaly and surface anomalous divergence to its west and northwest, as well as strong SLP zonal gradient along the equator (Fig. 6b), suggesting a southward shift of the Intertropical Convergence Zone (ITCZ) during these months in the central and eastern ocean. The shift of the wind direction is much weaker, and is seen only around the west of the dateline near Jan. (0) in the WP El Niño (Fig. 2a). Also, the precipitation and surface wind anomalies, and SLP zonal gradient, associated with the WP El

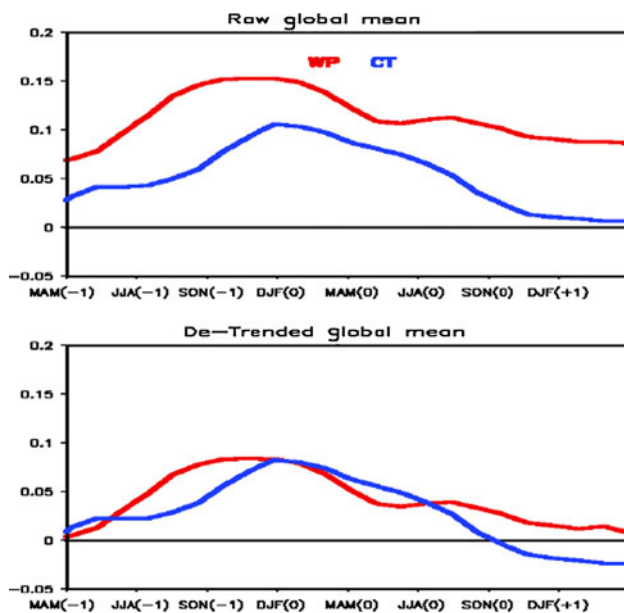


Fig. 9 Evolution of seasonal mean composites of globally averaged SSTA for the WP (red curve) and CT (blue curve) El Niño events with raw (top panel) and detrended (bottom panel) data during 1950–2008. Area weight is used in computing the globally averaged SSTA

Niño are much weaker (Fig. 6a). The lack of strong air–sea interaction over the cold tongue/ITCZ complex, as well as a lack of strong oceanic variability near the thermocline throughout its life cycle clearly differentiates WP events from the composite CT events. This is consistent with the composite results of Ashok et al. (2007) (see their Figs. 6–8), Kug et al. (2009), and Kao and Yu (2009).

To summarize, weak and westward confined (strong and eastward extended) westerly wind prior to the development of a warm event is associated with weak (strong) subsurface OTA as well as insignificant (active) air–sea interaction. Such differences lead to an emerging El Niño into development of a WP or a CT event. A question is why the thermocline feedback is not prominent in the WP events? One possibility is as follows: strong and eastward located westerly (Fig. 3b) and substantial SSTA (Fig. 2b) appearing in the eastern Pacific Ocean in boreal spring and early summer suppresses the seasonal enhancement of the cold tongue, and is a major factor in triggering the thermocline feedback and further development of CT events. In contrast, if the westerly is weak and located westward (Fig. 3a) and the SSTA (Fig. 2a) are absent in the eastern Pacific, and once the cold tongue is fully developed in boreal fall, it is difficult to disturb it. Moreover, once the growth of SSTA in the central Pacific is larger than, and precedes that in the eastern Pacific, as in most WP events, the anomalous SST and associated convection as well as the associated zonal wind in the eastern Pacific, are not conducive for the positive SSTA

growth in the east due to the weakened westerly anomaly there (Fig. 6a). Therefore, there is a competition between the initial amplitude of the SSTA in the eastern and western Pacific for the eventual fate of a developing warm event, and the winner usually determines the type of event. However, this hypothesis needs to be verified through theoretical study and model experiment.

3.2 Evolution of global SSTA

The differences of the amplitude, location, and evolution of seasonal mean SSTA in the tropical Pacific between the WP and CT El Niños (Fig. 7) are consistent with that shown in Fig. 2. The meridional contrast of the SSTA is compared by the zonal mean of respective composites (left column of Fig. 8). As such, the warming in the tropics is narrower in the meridional direction in the CT El Niño than in the WP El Niño. In the higher latitudes, the cooling in the subtropics of the Northern Hemisphere (NH) is larger and the warming in high latitudes of both hemispheres is smaller in the CT El Niño than in the WP El Niño. Due to the cancelation of the positive and negative anomalies, the global mean SSTA is in fact smaller for the CT El Niño than for the WP El Niño (top panel of Fig. 9).

The global oceans have experienced warming trends (Kumar et al. 2010), and to understand the extent warming trends may be influencing the composites, we also compare composites based on the detrended SSTA. A marked decrease in the amplitudes of the positive SSTA in the tropics and high latitudes of NH is evident for the WP El Niño for the detrended data (bottom right of Fig. 8 and bottom panel of Fig. 9). On the contrary, the impact of using detrended data on the CT El Niño composite is relatively smaller (top right of Fig. 8 and bottom panel of Fig. 9). It is also interesting to note that after detrending the amplitude of global mean SSTA for the WP and CT El Niños is of similar magnitude (bottom panel of Fig. 9). This suggests that the WP El Niño was associated with a relatively homogenous warming of the global oceans.

Besides the contrasts in the amplitude and the distribution pattern of the global SSTA, some other differences are also seen in the composites of the WP and CT El Niños. For example, the development of global SSTA is more gradual for the WP El Niño than for the CT El Niño (Fig. 9). There is a broader peak of global SSTA for the WP El Niño extending from SON (−1) to D(−1)JF(0), while the peak is sharper for the CT El Niño because of a sharper decay following its maximum in D(−1)JF(0). This difference is seen for both raw and detrended data. After detrending, colder SSTs occur in following boreal winter after the peak for the CT El Niño, but SSTs stay warmer for the WP El Niño, suggesting that the CT El Niño is associated with a stronger cycle in the global SSTA.

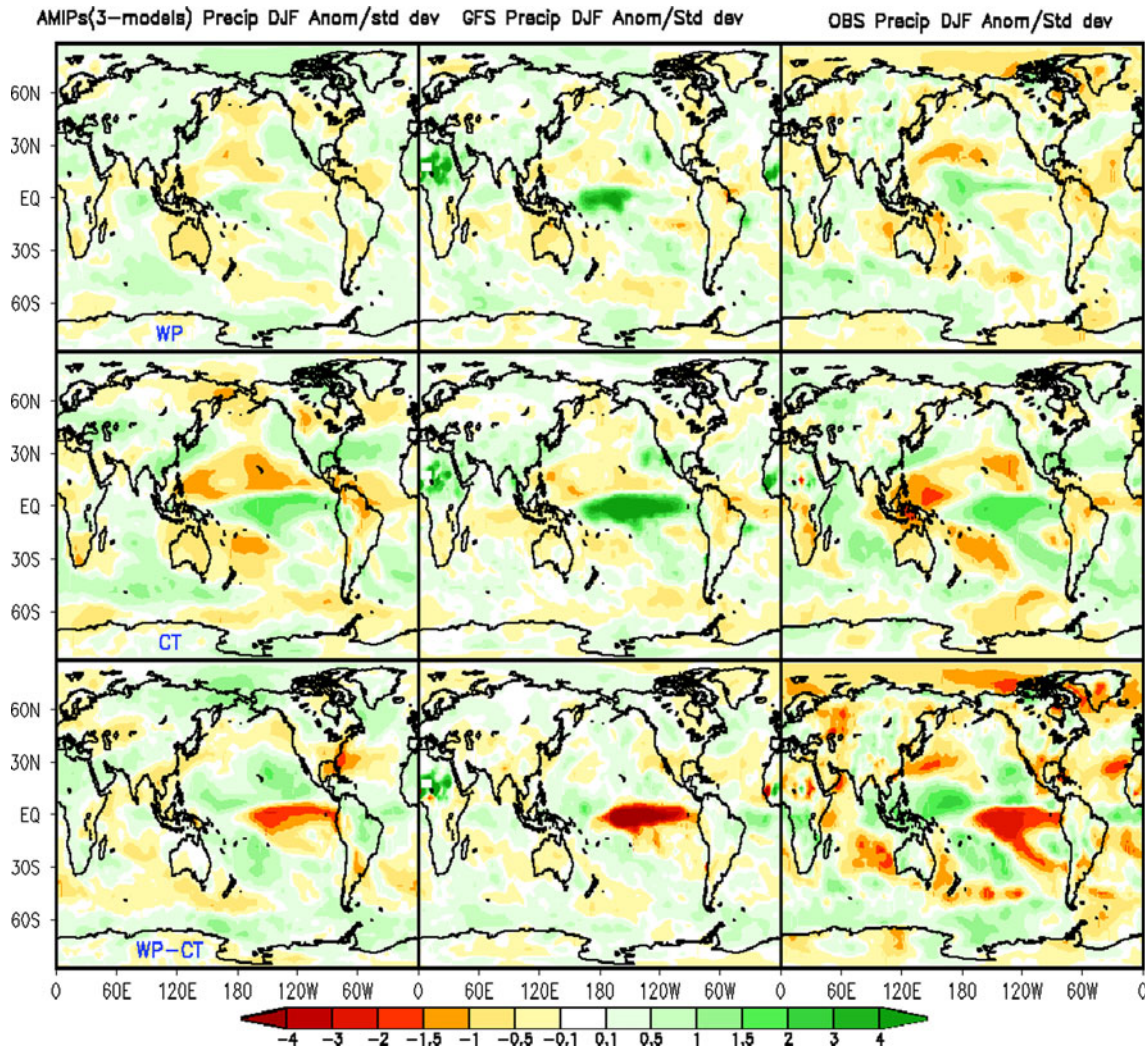


Fig. 10 Standardized precipitation anomaly (anomaly divided by its standard deviation) composites in $D(-1)JF(0)$ in 1979–2008. *Left column* three AGCMs (ECHAM4.5, NSIPP, and SFM) forced by observed SST during 1979–2008. *Central column* 35 year integrations of the GFS forced by permanent and idealized SSTA in

$D(-1)JF(0)$ shown in Fig. 7. *Right column* CAMS-OPI during 1979–2008. *Top, middle, and bottom panels* in each column are the composites of the WP El Niño, the CT El Niño and the difference between them, respectively

4 Extra-tropical response and hindcast skill of WP and CT El Niño

As the amplitude and spatial distribution of SSTA between WP and CT differs, it is natural to anticipate that the respective atmospheric responses will also be different. In this section, to identify the robust differences in the atmospheric response between WP and CT El Niños, we examine AMIP type simulations and compare with the corresponding observations. We focus on the analysis of precipitation and land surface air temperature in $D(-1)JF(0)$, since the signals in boreal winter are strongest compared with other seasons (particularly in NH), although an analysis for this season may slightly undermine the effects of the WP events because they peak in Nov.–Dec. and the CT events in Dec.–Jan. (Fig. 2). Furthermore, we also compare the differences of the

prediction skill for tropical Pacific SSTA between the WP and CT El Niños using CFS hindcasts.

4.1 Global precipitation and surface air temperature response

The standardized total precipitation anomaly composites in $D(-1)JF(0)$ are displayed in Fig. 10 using the data from Jan. 1979 to Dec. 2008 for the AMIP runs (left column) and observations (right columns), and for 35-year integrations of GFS sensitivity experiments (central column). Although there are some similarities in the global pattern of precipitation response, observed precipitation composites also show important differences between the WP and CT El Niños, which are generally consistent with the corresponding regression patterns shown in Fig. 4 of Weng et al.

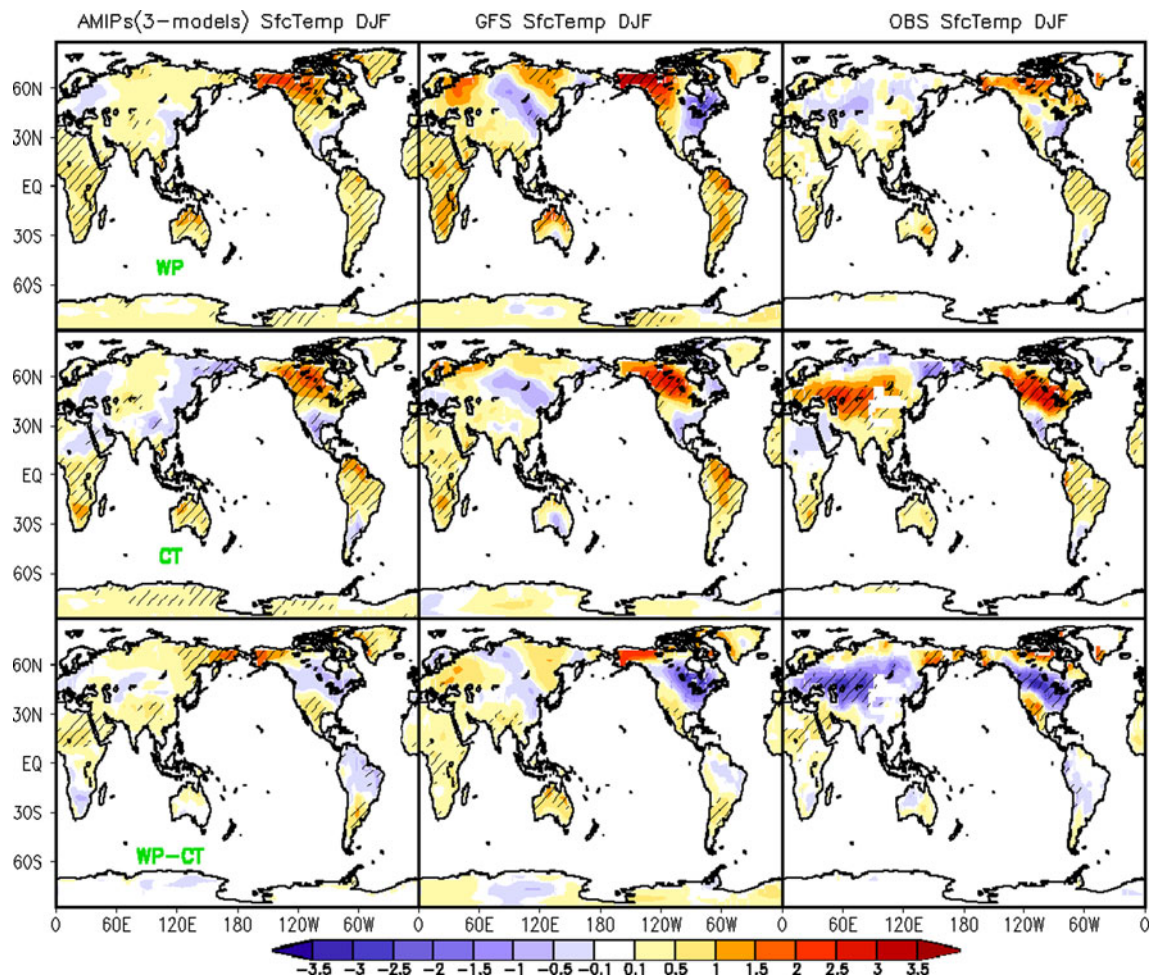


Fig. 11 Land surface air temperature anomaly composites in $D(-1)JF(0)$. *Left column* integrations of three AGCMs (ECHAM4.5, NSIPP, and SFM) forced by observed SST during 1950–2008. *Central column* 35 year integrations of the GFS forced by permanent and idealized SSTA in $D(-1)JF(0)$ shown in Fig. 7. *Right column*

CAMS during 1950–2008. *Top, middle, and bottom panels* in each column are the composites of the WP El Niño, CT El Niño and the difference between them, respectively. The regions with *slant lines* show the significant anomaly or difference at the level of 95% using the *T* test

(2009), particularly in the tropical Pacific (right columns of Fig. 10). Both types of El Niño events cause an eastward displacement of the precipitation over the equatorial Pacific. However, consistent with the tropical SSTA pattern (Fig. 7), the center of positive anomalous precipitation is located in the western and central Pacific in the WP El Niño, while it is shifted into the central and eastern Pacific in the CT El Niño. Compared with the CT El Niño, the WP El Niño causes less precipitation in the eastern equatorial Pacific and more precipitation in the northwestern tropical Pacific and the South Pacific Convergence Zone.

Overall patterns of the observed precipitation anomalies in the WP and CT El Niños in the tropical Pacific are captured well in both the AMIP runs and GFS sensitivity experiments (top and middle panels of Fig. 10). Furthermore, the east-west gradient contrast between the WP and CT El Niños in the tropical Pacific is also well simulated, although the positive anomalies are underestimated in the

tropical northwestern and southwestern Pacific (bottom panels of Fig. 10). In addition, the contrast in the tropical Indian Ocean, tropical Atlantic Ocean, and North America between the WP and CT El Niños is generally well simulated.

The land surface air temperature anomaly composites in $D(-1)JF(0)$ (with their significance) are shown in Fig. 11 using the data from Jan. 1950 to Dec. 2008 for the AMIP simulations (left column) and observations (right columns), as well as 35-year integrations from the GFS (central column). The overall anomalous pattern in the observations (right columns of Fig. 11) is similar to the corresponding regression pattern shown in Fig. 3 of Weng et al. (2009). In general, the observed land surface temperature anomaly patterns of both the WP and CT El Niños are reasonably well simulated in the AMIP runs and GFS sensitivity experiments, particularly in the tropics, North and South American, and African continents.

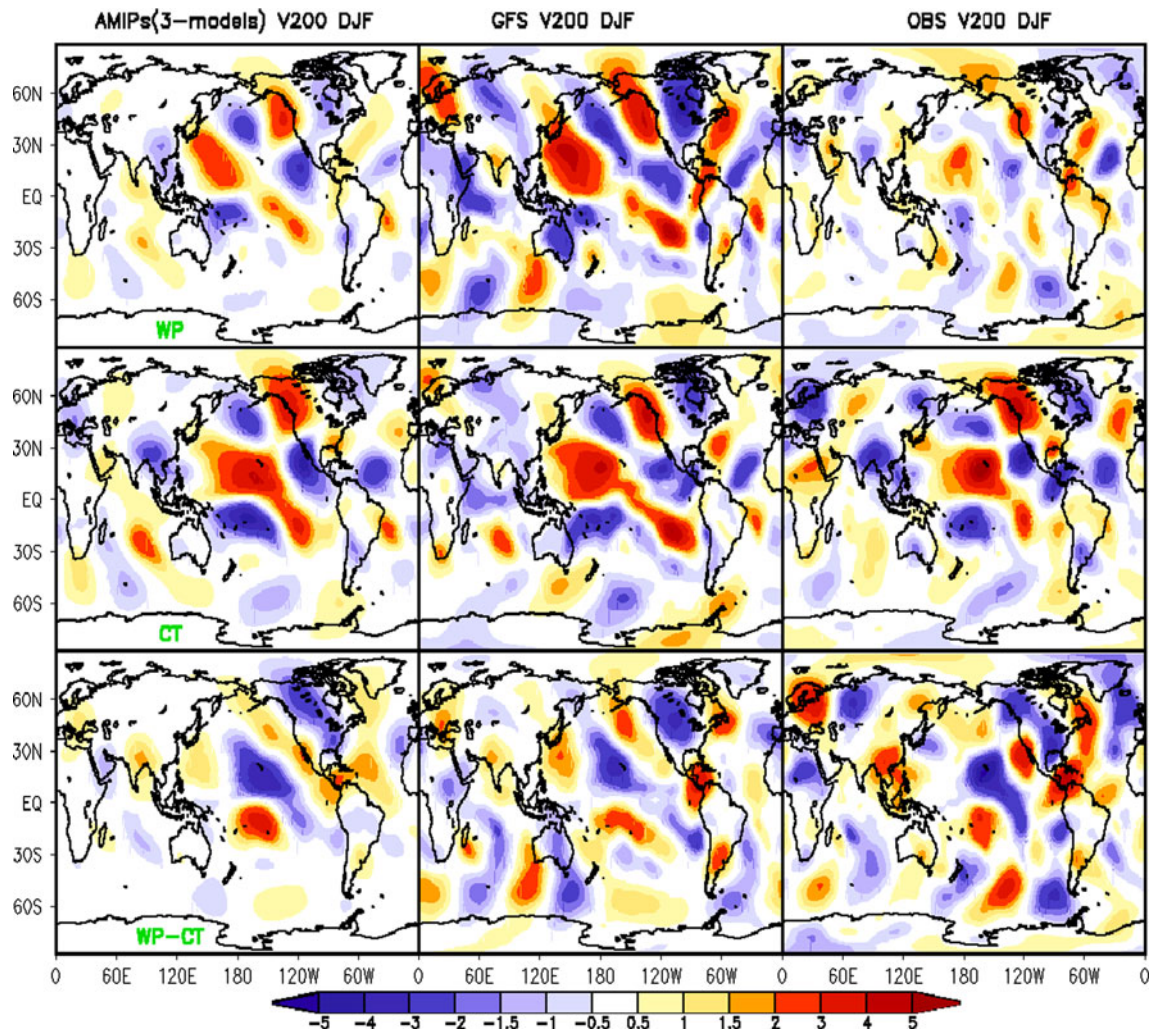


Fig. 12 200 hPa meridional wind anomaly composites in $D(-1)JF(0)$. *Left column* three AGCMs (ECHAM4.5, NSIPP, and SFM) forced by observed SST during 1950–2008. *Central column* 35 year integrations of the GFS forced by permanent and idealized

SSTA in $D(-1)JF(0)$ shown in Fig. 7. *Right column* R1 during 1950–2008. *Top, middle, and bottom panels* in each column are the composites of the WP El Niño, the CT El Niño and the difference between them, respectively

Both the AMIP runs and GFS sensitivity experiments, however, do not reproduce the observed contrast of land surface air temperature anomalies in the Eurasian continent between the two types of El Niños. Observationally, patterns with opposite signs are seen in the WP and CT El Niños in the area, but no such reversal is found in the model simulations. This discrepancy may imply that the surface air temperature anomalies over the Eurasian continent are not significantly affected by the type of El Niños, and the observed anomalies, although statistically significant, are an artifact of sampling variability. Another possibility is that models are indeed unable to reproduce the contrast in the regions. Analysis of simulations based on other models, or with longer observational data record, will help clarify this issue.

Differences in remote response are likely associated with differences in the stationary wave propagation forced

by tropical heating anomalies that occur in different locations in the two types of El Niños (Fig. 12) (Kumar et al. 2005; Weng et al. 2009). To investigate this, we follow the approach of Jin and Hoskins (1995) and analyze the anomaly meridional component of wind at 200 hPa (v_{200}) to track the stationary wave propagation. Consistent with Fig. 9 of Weng et al. (2007) and Fig. 8 of Weng et al. (2009), there are two major teleconnection patterns: PJ and PNA in NH associated with El Niño (Fig. 12). On average, the observed v_{200} response is weaker in the WP than in the CT El Niños, likely due to the intensity difference of the tropical SSTA and corresponding precipitation response. Corresponding to the westward displacement of the tropical convection (precipitation, see right column of Fig. 10) between the WP and CT El Niños, the PNA pattern is shifted in the observations (see right column of Fig. 12). For example, the positive v_{200} anomalies in the central

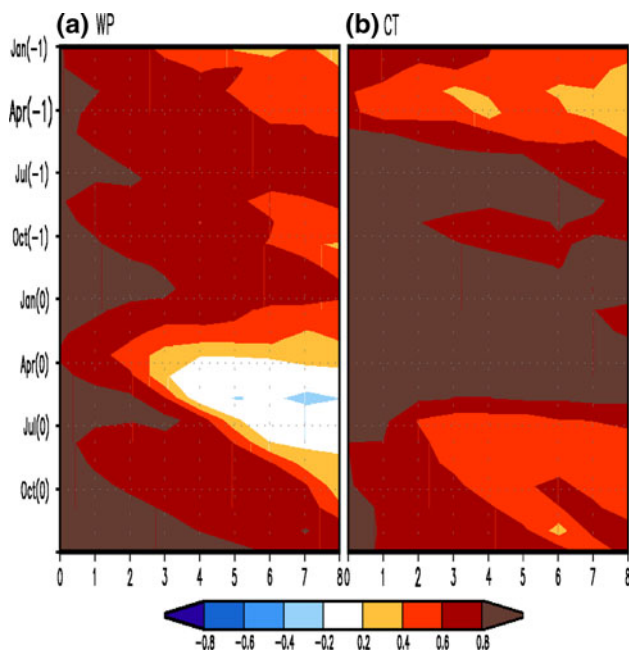


Fig. 13 Pattern correlations between observed and CFS predicted SSTA in 10°S – 10°N and 120°E – 100°W in the **a** WP and **b** CT El Niño years during 1981–2009 varied with months of initial conditions (y-axis) and lead months (x-axis)

subtropical Pacific, and the negative ones to the south, are in a westward location and the negative and positive anomaly centers in North America are shifted southward in the WP El Niño (central right panel of Fig. 12). The changes in the surface air temperature over North America may be a consequence of the location shift and intensity difference of the tropical forced anomalous ridge over North America that causes different cold and warm air advectations between the CT and WP El Niños.

The general patterns of v200 anomalies in the WP and CT El Niños composites, and their contrasts seen in the observations (right column of Fig. 12), are reproduced in both the AMIP runs and GFS sensitivity experiments (left and central columns of Fig. 12), particularly in the eastern Pacific, North America and North Atlantic. Nevertheless, the contrasts of the anomalies of v200 over the Eurasian continent between the WP and CT El Niños are underestimated in the model simulations. Also, the amplitudes of the anomalies in the WP El Niño composite are overestimated in these simulations, particularly in the GFS sensitivity experiments.

Overall, the model simulations and sensitivity experiments suggest that the contrasts in the atmospheric response between the WP and CT El Niños in the eastern Pacific, North America and North Atlantic are robust, and are largely due to the displacement in path of stationary wave propagation caused by the shift of tropical Pacific heating source. The contrast in the observed surface

temperature over the Eurasian continent is not replicated in model simulations and may not be directly connected to the two types of El Niño.

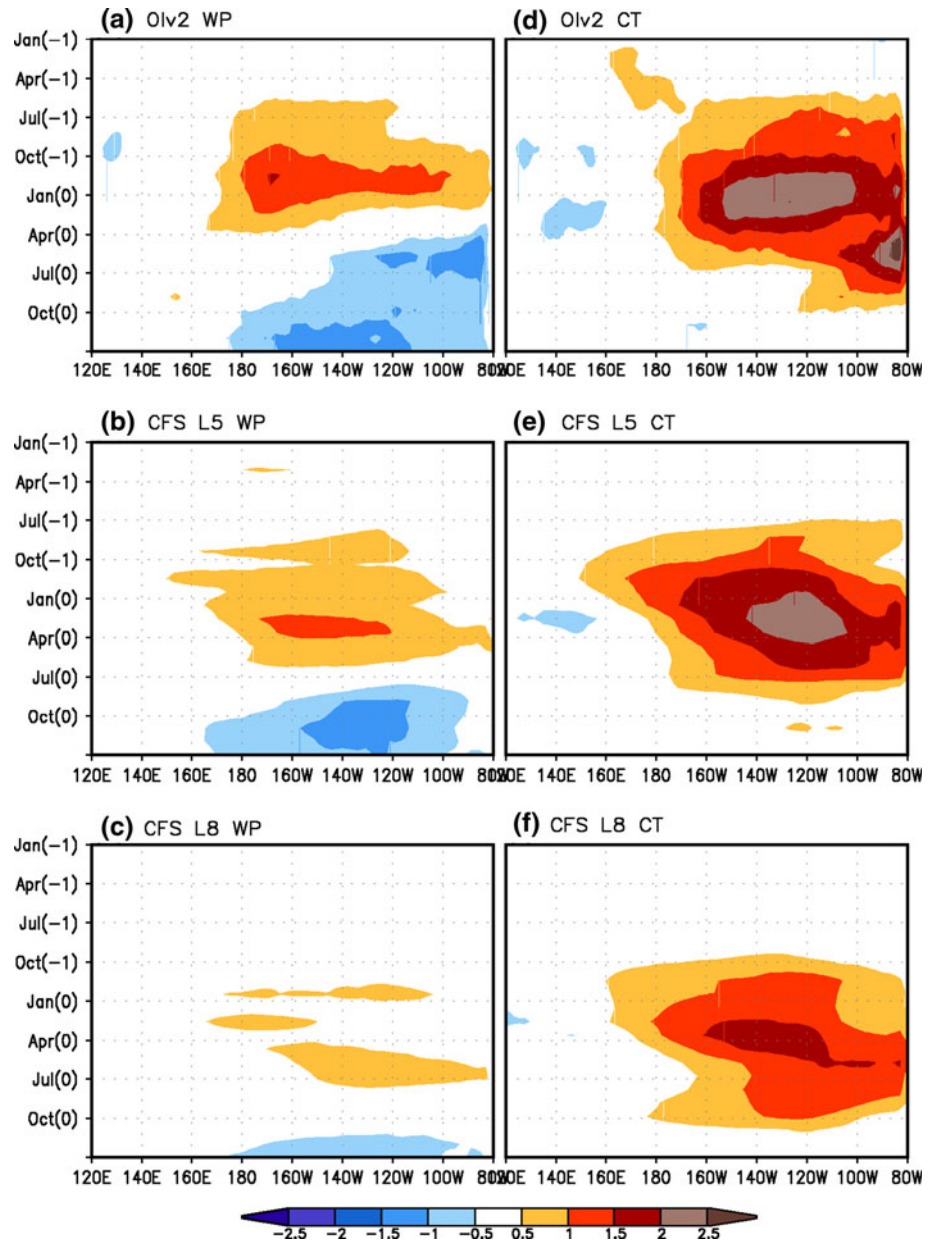
4.2 Hindcast skill in the CFS

Figure 13 shows the pattern correlation between observed and CFS predicted SSTA in 10°S – 10°N and 120°E – 100°W in the (a) WP and (b) CT El Niño years during 1979–2009 as a function of calendar month of the IC and forecast lead time. On average, the hindcast skill is lower for the WP El Niño events than for the CT El Niño events. Furthermore, for WP El Niño, the hindcast skill is less affected by the so-called “spring barrier” in its developing phase (see the minimum in Apr. (–1) ICs in Fig. 13a) than in its decaying phase (see the minimum in Apr. (0) ICs in Fig. 13a).

There are also some other differences in predicting the SSTA evolution between the WP and CT El Niños (Fig. 14). For the WP El Niño (left column), the SSTA amplitude peaks later in Feb. (0)–Mar. (0) in the CFS hindcasts for 5 month lead predictions (Fig. 14b) compared to Nov. (–1)–Dec. (–1) in the observations (Fig. 14a). A cooling occurs immediately in the summer following winter in the observations and in autumn following winter in the hindcasts with 5 month lead. Consistent with the hindcast skill difference in Fig. 13, the CFS is more skillful in predicting SSTA evolution in the CT El Niño than in the WP El Niño (Fig. 14). Both the amplitude of SSTA in the peak phase of the CT El Niño, and the persistence of the positive SSTA are well hindcast, even with 8 month lead. However, there is a similar delay for the peak phase in the hindcasts for both the WP and CT El Niños. Also, there is almost no propagation in the composite of predicted SSTA in the CT El Niño, while the westward propagation is visible in the observations. We should also point out that the classification of WP and CT events in the CFS hindcasts is based on that of observed SSTA shown in Fig. 1, which may be affected by the model biases.

The higher hindcast skill for the CT events than for the WP events may be due to the fact that the amplitude of SSTA in the Niño3.4 region is larger in the former than in the later (see Sect. 3). This result is consistent with Kumar (2009) and Wang et al. (2010). Wang et al. (2010) argued that the SST forecast skill in the eastern and central tropical Pacific in the CFS is a function of the amplitude of inter-annual variability of tropical Pacific SST: larger (smaller) variability of SSTA corresponding to higher (lower) skills of SSTA hindcast in the Niño3.4 region (see their Fig. 5). The higher hindcast skill in the CT El Niños than in the WP El Niños may also be due to the fact that preceding signal of surface westerly wind and subsurface ocean temperature as well as the air-sea interaction (Figs. 2, 3, 4, 5, 6) are

Fig. 14 SSTA composites of (a, d) observed, CFS hindcast with (b, e) 5 month lead and (c, f) 8 month lead for the WP (left column) and CT (right column) El Niño years during 1981–2009 varied with targeted months (y-axis) and longitudes (x-axis)



stronger and more substantial in the former than in the later.

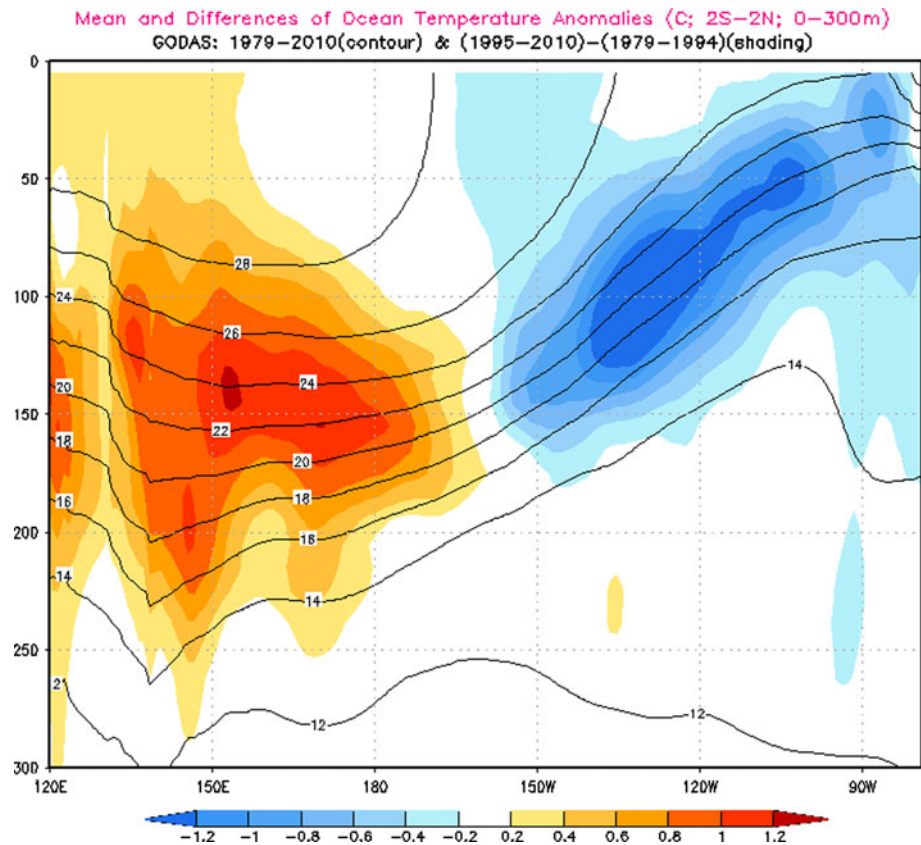
5 Long-term variation and possible explanation

It has been shown that the frequency of the WP El Niño may have increased in recent decades (Yeh et al. 2009; Lee and McPhaden 2010). Also, some analyses of climate change projection simulations suggest that the frequency of the WP El Niño will become more significant in global warming scenario (Yeh et al. 2009). Such low-frequency changes in the ENSO characteristics may be related to changes in the equatorial mean state of the ocean.

Therefore, it is interesting to explore the low frequency variations of atmosphere and ocean conditions and their possible connection with the changes of ENSO.

Figure 15 shows the mean and two period difference of ocean temperature along the equator. The positive difference in the west and negative one in the east along the thermocline indicates an increase of the thermocline tilt along the equator during 1979–2010. This result is different from previous results about the trend of thermocline depth. This disagreement may be caused by the fact that data from different sources and different periods were used. For example, Ashok et al. (2007) discussed a relative flattening trend of the thermocline tilt by comparing the means for 1956–1979 and 1980–2004 (see their Fig. 17c).

Fig. 15 Mean (*contour*) and difference (*shading*) of GODAS ocean temperature averaged between 2°S and 2°N. The mean is the average in 1979–2010, and the difference is the mean in 1995–2010 minus the mean in 1979–1994. Contour interval is 2°C



Actually, for the low frequency part with time scales longer than 6 years, the former period (1956–1979) corresponds to positive anomalies of HC300 in the western and negative ones in the eastern Pacific, and the later period (1980–2004) is tied with a similar pattern with opposite sign (Fig. 16b). Thus, the thermocline differences shown in Ashok et al. (2007) (see their Fig. 17c) may primarily reflect an interdecadal variation instead of trend in the tropical Pacific. In fact, some WP El Niños (1988, 1995) occurred in an anomalously flattened thermocline period, and some (1969, 2003, 2007) in an anomalously sharp thermocline period (Fig. 16b). Thus, it is arguable that if the recent flattening of thermocline trend can be used to explain the frequency increase of the WP El Niño in the recent decade (Ashok et al. 2007; Kao and Yu 2009; Yeh et al. 2009), and the association between the two remains an open question.

6 Discussion and conclusions

In this work, we use observed and (re)analyzed data as well as model simulations and hindcasts to (1) examine the differences of intensity and location of preceding westerly associated with the air-sea interaction and its role in

tropical air-sea interaction processes between the WP and CT El Niños, (2) identify the robust differences of the extra-tropical responses, (3) compare the hindcast skill differences between the two types of El Niños using NOAA CFS hindcasts, and (4) explore the low frequency variations of atmosphere and ocean conditions in the recent decades and their possible connection with the change of ENSO.

Consistent with previous results, such as Ashok et al. (2007), our individual case study and composite results show that strong (weak) and eastward located westerly wind along the equator preceding El Niño may result in active (weak) air-sea interaction over the cold tongue/ITCZ complex, and strong (weak) thermocline feedback, favoring the development of a CT (WP) El Niño. The differences of location and intensity of the westerly winds may affect the seasonal enhancement of the cold tongue and result different type of El Niño development. The WP and CT El Niños also have different time evolution and intensity of global SSTA. On average, SSTA in the tropical eastern Pacific in the CT El Niño is larger than that in the WP El Niño. The warming in the tropics is narrower in the meridional direction in the CT El Niño than in the WP El Niño. In the extra-tropics, the cooling in the subtropics of the NH is larger and the warming in high latitudes of both

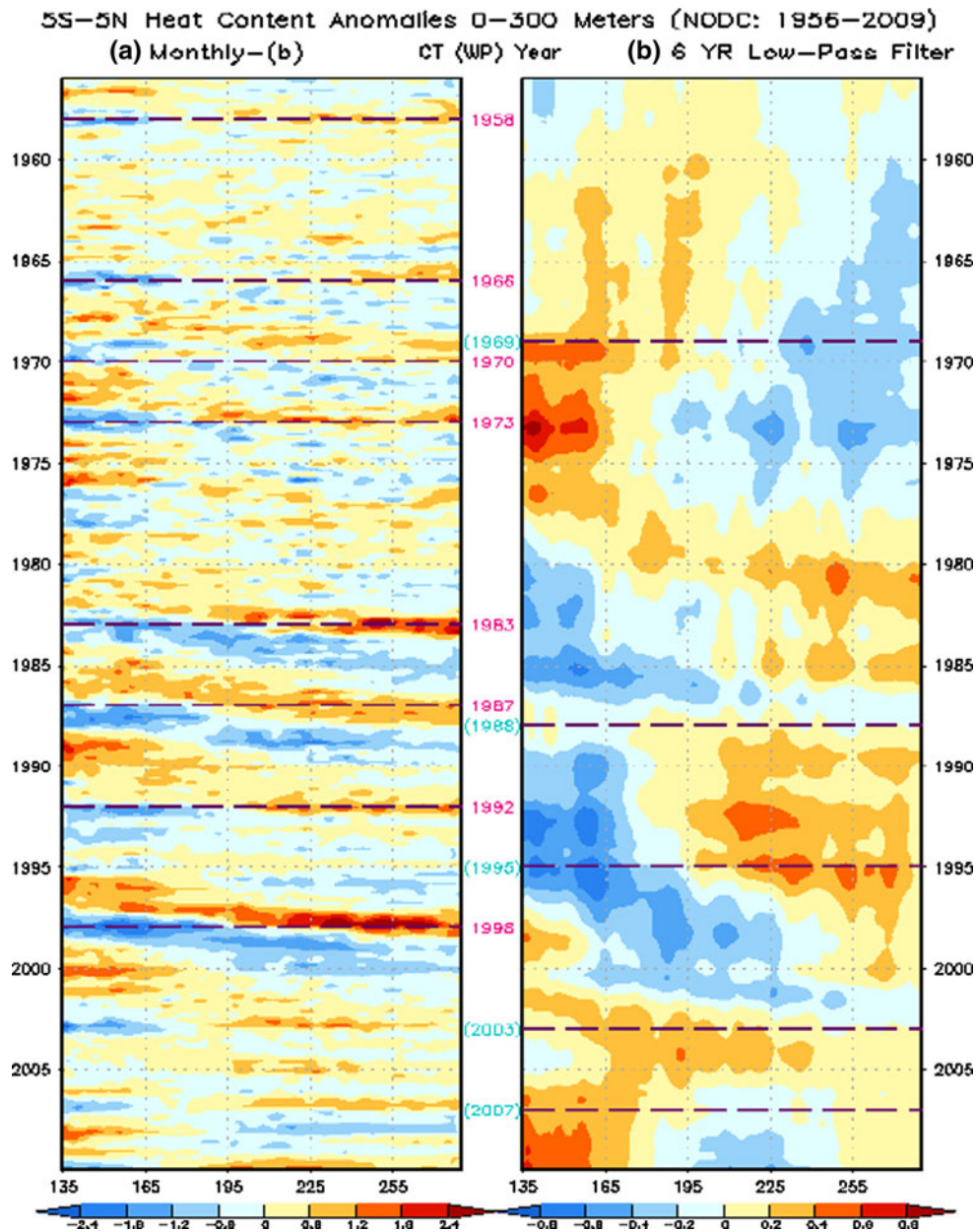


Fig. 16 NODC monthly mean heat content anomalies (mean temperature anomalies between the ocean surface and 300 m) averaged in 5°S–5°N in 1956–2009. **b** is the lower-pass filtered part after applying 73 month running mean, and **a** is the higher frequency part, which is the differences between raw data and **(b)**. The CT (WP) El Niño years

are marked (marked with *bracket*) in the middle between *two panels* and are represented by *horizontal dashed lines* in the left (right) column. These *horizontal dashed lines* are drawn in Jan. of El Niño years

hemispheres is much smaller in the CT than in the WP El Niño. As a result, the global averaged SSTa at their peak phase is even larger in the WP than in the CT El Niño.

The WP and CT El Niños show robust differences in the atmospheric responses. In addition to the tropics, the eastern Pacific, North America and North Atlantic are the major regions having robust climate differences between the WP and CT El Niños. The different responses are consistent with the displacement of the stationary wave

propagation path due to the zonal location difference of tropical Pacific heating source in the two types of El Niños. Nevertheless, the climate contrasts over the Eurasian continent seems not robust.

The differences of signal to noise ratio and some preceding signals, such as difference of surface westerly wind location and intensity, as well as air-sea interaction between the two events prior to their development may also explain differences in hindcast skills of tropical Pacific

SSTA between WP and CT El Niños. In the NCEP CFS, on average, the hindcast skill is lower for the WP El Niño than for the CT El Niño. However, the robustness of differences in hindcast skill need to be substantiated based on other coupled prediction systems.

The deepening (shoaling) of thermocline in the western (eastern) Pacific suggests a *sharper thermocline tilt* along the equator in recent decades. Shaper thermocline tilt is also consistent with changes in SSTAs. The change in thermocline, therefore, is different from previous results that pointed to a flattening trend, and might be due to using data from different periods. We also point out that some WP El Niños occurred in an anomalously flattened thermocline period, and some presented in an anomalously sharp thermocline period. Therefore, the frequency increase of the WP El Niño in the recent decade may not have a causal link with the change of thermocline depth in the equatorial Pacific.

Some caution should be exercised in the interpretation of the results. First, the results based on the observational composites, may be not robust due to the small sample size. Further accumulation of new observations will lead to further clarification. Second, some El Niño events may show both CT and WP characteristics at different stages of evolution. As a result, classification of El Niños may depend on what criteria and dataset are used. For example, using the DJF Nino3, Nino4 and their difference as measurements, the 1992/1992 event was defined as an EP (CT) event here. But it was classified as a WP event in Kug et al. (2009) when using a broader seasonal mean from Sep. to the following Feb. An examination of this particular event shows that after an eastward propagating signal in early spring, the SSTA and the wind anomalies were generally larger in the central Pacific from boreal summer to fall. However, an eastward surge did occur in late fall, which generated the warm SSTA in boreal winter season. This kind of late CT development also needs further analysis in future.

Acknowledgments We appreciate the comments, suggestions, and helps from Michelle L'Heureux, Kingtse Mo, Peitao Peng, and Mingyue Chen, as well as two anonymous reviewers, which largely improved the manuscript. Bohua Huang is supported by the NOAA CVP Program (NA07OAR4310310) as well as the COLA omnibus program from NSF, NOAA, and NASA.

References

- Ashok K, Behera SK, Rao SA, Weng H, Yamagata T (2007) El Niño Modoki and its possible teleconnection. *J Geophys Res* 112:C11007. doi:10.1029/2006JC003798
- Bacmeister JT, Pegion PJ, Schubert SD, Suarez MJ (2000) An atlas of seasonal means simulated by the NSIPP 1 atmospheric GCM. 17, NASA Goddard Space Flight Center Tech. Memo. 104606, p 194
- Behringer DW, Xue Y (2004) Evaluation of the global ocean data assimilation system at NCEP: The Pacific Ocean. In: Eighth symposium on integrated observing and assimilation systems for atmosphere, oceans, and land surface, AMS 84th annual meeting, Seattle, Washington, 11–15
- Bjerknes J (1969) Atmospheric teleconnections from the equatorial Pacific. *Mon Weather Rev* 97:163–172
- Choi J, An S-I, Kug J-S, Yeh, S-W (2011) The role of mean state on changes in **El Niño's flavor**. *Clim Dyn*. doi:10.1007/s00382-010-0912-1 (published online)
- Giese BS, Harrison DE (1990) Aspects of the Kelvin wave response to episodic wind forcing. *J Geophys Res* 95:7289–7312
- Harrison DE, Chiodi AM (2009) Pre- and post 97/98 westerly wind events and equatorial Pacific cold tongue warming. *J Clim* 22:568–581. doi:10.1175/2008JCLI2270
- Harrison DE, Vecchi G (1997) Surface westerly wind events in the tropical Pacific 1986–1995. *J Clim* 10:3131–3156
- Hoerling MP, Kumar A (2002) Atmospheric response patterns associated with tropical forcing. *J Clim* 15:2184–2203
- Huang B, Schneider EK (1995) The response of an ocean general circulation model to surface wind stress produced by an atmospheric general circulation model. *Mon Weather Rev* 123:3059–3085
- Huang B, Xue Y, Zhang D, Kumar A, McPhaden MJ (2010) The NCEP GODAS ocean analysis of the tropical Pacific mixed layer heat budget on seasonal to interannual time scales. *J Clim* 23:4901–4925
- Janowiak JE, Xie P (1999) CAMS-OPI: a global satellite-rain gauge merged product for real-time precipitation monitoring applications. *J Clim* 12:3335–3342
- Jin F-F, Hoskins BJ (1995) The direct response to tropical heating in a baroclinic atmosphere. *J Atmos Sci* 52:307–319
- Kalnay E et al (1996) The NCEP/NCAR 40-year reanalysis project. *Bull Am Meteorol Soc* 77:437–471
- Kanamitsu M et al (2002a) NCEP-DOE AMIP-II Reanalysis (R-2). *Bull Am Meteorol Soc* 83:1631–1643
- Kanamitsu M et al (2002b) NCEP dynamical seasonal forecast system 2000. *Bull Am Meteorol Soc* 83:1019–1037
- Kao H-Y, Yu J-Y (2009) Contrasting eastern-Pacific and central-Pacific types of ENSO. *J Clim* 22:615–632
- Kindle JC, Phoebus PA (1995) The ocean response to operational westerly wind bursts during the 1991–1992 El Niño. *J Geophys Res* 100:4893–4920
- Kug J-S, Jin F-F, An S-I (2009) Two types of El Niño events: cold tongue El Niño and warm pool El Niño. *J Clim* 22:1499–1515. doi:10.1175/2008JCLI2624.1
- Kug J-S, Choi J, An S-I, Jin F-F, Wittenberg AT (2010) Warm pool and cold tongue El Niño events as simulated by the GFDL 2.1 coupled GCM. *J Clim* 23:1226–1239
- Kumar A (2009) Finite samples and uncertainty estimates for skill measures for seasonal predictions. *Mon Weather Rev* 137:2622–2631
- Kumar A, Hu Z-Z (2011) Uncertainty in the ocean-atmosphere feedbacks associated with ENSO in the reanalysis products. *Clim Dyn*. doi:10.1007/s00382-011-1104-3 (published online)
- Kumar A, Zhang Q, Peng P, Jha B (2005) SST-forced atmospheric variability in an atmospheric general circulation model. *J Clim* 18:3953–3967
- Kumar A, Jha B, L'Heureux M (2010) Are tropical SST trends changing the global teleconnection during La Niña? *Geophys Res Lett* 37:L12702. doi:10.1029/2010GL043394
- Larkin NK, Harrison DE (2005) Global seasonal temperature and precipitation anomalies during El Niño autumn and winter. *Geophys Res Lett* 32:L13705. doi:10.1029/2005GL022738
- Latif M, Kleeman R, Eckert C (1997) Greenhouse warming, decadal variability, or El Niño? An attempt to understand the anomalous 1990 s. *J Clim* 10:2221–2239
- Lee T, McPhaden MJ (2010) Increasing intensity of El Niño in the central equatorial Pacific. *Geophys Res Lett* 37:L14603. doi:10.1029/2010GL044007

- Levitus S et al (2009) Global ocean heat content 1955–2008 in light of recently revealed instrumentation problems. *Geophys Res Lett* 36:L07608. doi:[10.1029/2008GL037155](https://doi.org/10.1029/2008GL037155)
- Luther DS, Harrison DE (1984) Observing long-period fluctuations of surface winds in the tropical Pacific: initial results from island data. *Mon Weather Rev* 112:285–302
- Luther DS, Harrison DE, Knox RA (1983) Zonal winds in the central equatorial Pacific and El Niño. *Science* 222:327–330
- Reynolds RW, Rayner NA, Smith TM, Stokes DC, Wang W (2002) An improved in situ and satellite SST analysis for climate. *J Clim* 15:1609–1625
- Roekner E et al (2006) Sensitivity of simulated climate to horizontal and vertical resolution in the ECHAM5 atmosphere model. *J Clim* 19:3771–3791
- Ropelewski CF, Janowiak JE, Halpert MS (1985) The analysis and display of real time surface climate data. *Mon Weather Rev* 113:1101–1106
- Saha S et al (2006) The NCEP climate forecast system. *J Clim* 19:3483–3517
- Smith TM, Reynolds RW, Peterson TC, Lawrimore J (2008) Improvements to NOAA's historical merged land-ocean surface temperature analysis (1880–2006). *J Clim* 21:2283–2296
- Trenberth KE, Smith L (2006) The vertical structure of temperature in the tropics: different flavors of El Niño. *J Clim* 19:4956–4973
- Wang W, Chen M, Kumar A (2010) An assessment of the CFS real-time seasonal forecasts. *Weather Forecast* 25:950–969. doi:[10.1175/2010WAF2222345.1](https://doi.org/10.1175/2010WAF2222345.1)
- Wang W, Chen M, Kumar A, Xue Y (2011) How important is intraseasonal surface wind variability to real-time ENSO prediction? *Geophys Res Lett* 38:L13705. doi:[10.1029/2011GL047684](https://doi.org/10.1029/2011GL047684)
- Weare BC, Navato AR, Newell RE (1976) Empirical orthogonal analysis of Pacific sea surface temperatures. *J Phys Ocean* 6:671–678
- Weng H, Ashok K, Behera SK, Rao SA, Yamagata T (2007) Impacts of recent El Niño Modoki on droughts/floods in the Pacific rim during boreal summer. *Clim Dyn* 29:113–129. doi:[10.1007/s00382-007-0234-0](https://doi.org/10.1007/s00382-007-0234-0)
- Weng H, Behera SK, Yamagata T (2009) Anomalous winter climate conditions in the Pacific rim during recent El Niño Modoki and El Niño events. *Clim Dyn* 32:663–674. doi:[10.1007/s00382-008-0394-6](https://doi.org/10.1007/s00382-008-0394-6)
- Yeh S et al (2009) El Niño in a changing climate. *Nature* 461:511–514
- Yu J-Y, Kim ST (2010a) Three evolution patterns of central-Pacific El Niño. *Geophys Res Lett* 37:L08706. doi:[10.1029/2010GL042810](https://doi.org/10.1029/2010GL042810)
- Yu J-Y, Kim ST (2010b) Identification of central-Pacific and eastern-Pacific types of ENSO in CMIP3 models. *Geophys Res Lett* 37:L15705. doi:[10.1029/2010GL044082](https://doi.org/10.1029/2010GL044082)